Modelled storm surge changes in a warmer world: the Last Interglacial

Paolo Scussolini[1,*], Job Dullaart[1], Sanne Muis[1,2], Alessio Rovere[3,4], Pepijn Bakker[5], Dim
5   Coumou[1], Hans Renssen[6], Philip J. Ward[1], and Jeroen C.J.H. Aerts[1,2]

[1]Institute for Environmental Studies, Vrije Universiteit Amsterdam, Amsterdam, The Netherlands

[2]Deltares, Delft, The Netherlands

[3]Department of Environmental Sciences, Informatics and Statistics, Ca' Foscari University of Venice, Italy

[4]MARUM, Center for Marine Environmental Sciences, University of Bremen, Germany

10   [5]Earth and Climate Cluster, Vrije Universiteit Amsterdam, Amsterdam, The Netherlands

[6]University of South-Eastern Norway, Bø, Norway

[*]Corresponding author: paolo.scussolini@vu.nl

Abstract. The Last Interglacial (LIG; ca. 125 ka) is a period of interest for climate research as it is the most recent

15 period of the Earth's history when the boreal climate was warmer than at present. Previous research, based on models and geological evidence, suggests that the LIG may have featured enhanced patterns of ocean storminess, but this remains hotly debated. Here, we apply state-of-the-art climate and hydrodynamic modeling to simulate changes in extreme sea levels caused by storm surges, under LIG and pre-industrial climate forcings. Significantly higher seasonal LIG sea level extremes emerge for the Gulf of Carpentaria, parts of Indonesia, the Mediterranean

20 Sea and northern Africa, the Gulf of Saint Lawrence, the Persian Gulf, Pakistan, northwest India, and islands of the Pacific Ocean and of the Caribbean. Lower LIG sea level extremes emerge for the Baltic and North Seas, the Bay of Bengal, China and Vietnam. Some of these anomalies are clearly associated with anomalies in seasonal sea level pressure minima, and potentially also originate from anomalies in the meridional position and intensity of the predominant wind bands. In a qualitative comparison, LIG sea level extremes seem generally higher than those

25 projected for future warmer climates. These results help to constrain the interpretation of coastal archives of LIG sea level indicators.

1 Introduction

Storm surges are temporary changes in sea level driven by strong winds and low atmospheric pressures (Resio and

30 Westerink, 2008). In combination with tides and waves, they are the main driver of sea level extremes along the world's coasts (Enríquez et al., 2020; Kirezci et al., 2020; Muis et al., 2016). The genesis and intensity of low-pressure systems depend on large-scale patterns of atmospheric circulation, on sea surface temperature, and on water vapor content of the low atmosphere. These processes that drive storm surges may adjust with ongoing climatic change. Climate reanalysis datasets of the last decades show signs of changes in the atmospheric circulation (Staten

35 et al., 2018) that are potentially due to global warming (e.g., Francis and Skific, 2015). These changes are expected to continue in the future, as sea surface temperatures (Bindoff, 2019) and water vapor content (Takahashi et al., 2016) are projected to increase. As a result, the region of tropical cyclone formation is expected to expand (Harvey et al., 2020), and the Atlantic coast of Europe may see more frequent landfall of tropical cyclones (Haarsma et al., 2013). Ensembles of climate models project a future poleward shift of boreal extra-tropical cyclones, and a decrease

40 in their occurrence (Chang et al., 2012). For the boreal mid-latitudes, the most recent generation of global climate models associate future global warming with a southern shift of winter storm tracks, and weakening of summer storm tracks (Harvey et al., 2020). However, projections of both tropical and extra-tropical cyclone occurrence remain contentious (Catto et al., 2019; Shaw et al., 2016; Yamada et al., 2017).

To understand the implications of different climate states on the occurrence of storm surges, we can look at past

45 periods in earth's history, for example during the warmer conditions of the Last Interglacial (LIG). Since geological proxies do not have the stratigraphic and temporal resolution needed to address storms and cyclones directly, a proposed method to examine these phenomena in the past is climate modelling (Raible et al., 2021). For example, by modeling a set of starkly different past climatic conditions, Koh and Brierley (2015) reveal that the potential for

generation of tropical cyclones only changes regionally. Specifically for the LIG, Kaspar et al. (2007) found a

50   strengthening of the winter mid-latitude storm tracks, along with a northward shift and an extension to the east.

1.1 The Last Interglacial

One period of particular interest for paleoclimate sciences is the Last Interglacial, spanning from 129 to 116 ka. This was the last period of the Earth's past when large parts of the globe were characterized by a climate slightly warmer than at present, at least in the Northern Hemisphere (CAPE_Members, 2006; Hoffman et al., 2017; McKay et al.,

55   2011; Shackleton et al., 2020; Turney et al., 2020b; Turney and Jones, 2010). On average, LIG polar temperatures were several degrees higher than pre-industrial (Jouzel et al., 2007; Neem_Community_Members, 2013), and ice sheets were smaller (Rohling et al., 2019; Turney et al., 2020a), with sea levels higher than today (Dutton et al., 2015a; Dutton et al., 2015b; Dyer et al., 2021; Kopp et al., 2009). Although key differences in the forcing of LIG and future climates prevent the use of the LIG as a direct analog for the future (Lunt et al., 2013; Otto-Bliesner et al.,

60   2013), its similarity with projected future thermal changes in some regions (especially the Northern Hemisphere) makes it a relevant process-analog for warmer climate conditions.

To date, patterns of LIG storminess are much less explored than temperature, ice sheet, and sea-level. Hansen et al. (2016) suggested that the (late) LIG may have been characterized by anomalous storminess in the Atlantic, and more generally in the subtropics. The notion of higher storminess is rooted in geological observations of so-called

65   "superstorm" deposits emplaced during the LIG along the coasts of the Bahamas (Hearty, 1997; Hearty et al., 1998) and Bermuda (Hearty and Tormey, 2017). These are large boulders and storm ridges whose size and position suggest that they were deposited by storms of higher intensity than recorded in human history. However, there are still debates around the origin of these proxies (Mylroie, 2008, 2018; Vimpere et al., 2019) and the type of storm that created them (Hearty and Tormey, 2018; Rovere et al., 2017; Rovere et al., 2018; Scheffers and Kelletat, 2020).

70   Recent modeling work has shown that the LIG might have seen higher-than-today sea surface temperatures, and more frequent and stronger tropical cyclones over the western North Atlantic (Yan et al., 2021). From proxies, reconstructions of storminess are only indirect, and are inferred from variables linked to storm tracks, such as precipitation (Scussolini et al., 2019) and river runoff (Scussolini et al., 2020), and seasonal gradients in precipitation and temperature (Salonen et al., 2021). Possible changes in LIG storm tracks might affect the

75   probabilities of storm surges at the coastline, but this effect has not been quantified.

1.2 Application of modeling to LIG storm surges

Compared to previous generations, the present generation of General Circulation Models (GCMs) is much more capable of simulating present-day boreal storm tracks and jet stream (Belmonte Rivas and Stoffelen, 2019; Dullaart et al., 2020; Roberts et al., 2020), with a reduction of almost 50% in root-mean-square error (Harvey et al, 2020).

80   However, GCMs still have a positive bias in the intensity, and a southern bias in the position of the zonal winds associated with summer storm tracks (Roberts et al., 2020). Further, the intensity of the strongest tropical cyclones seems to still be underestimated (ibid.). GCMs indicate significant changes in storm tracks under different climate change scenarios (Haarsma et al., 2013; Harvey et al., 2020), possibly resulting in a poleward shift in areas of

85   cyclone activity (Mori et al., 2019), and implying that future changes in storminess may contribute to higher coastal
sea level extremes (Vousdoukas et al., 2018).

In this paper, we explore the influence of the LIG atmospheric climate on global patterns of storm surges. We
examine changes in storm surge levels between climates of the LIG and the Pre-Industrial (PI), and link them to
changes in mean and extremes of atmospheric circulation. To achieve this, we employ meridional and zonal wind
speed and sea level pressure from simulations of LIG and PI climate with a global climate model to force a global

90   hydrodynamic model to simulate the extreme water levels along coastlines resulting from storm surges.

2   Methods

2.1   Climate simulations

The LIG and PI climates are simulated with the state-of-the-art coupled climate model CESM, version1.2 (Hurrell et
al., 2013). The model includes the Community Atmosphere Model (CAM5), Community Land Model (CLM4.0),

95   the Parallel Ocean Program (POP2.1), and the Community Ice Code (CICE4). We use a horizontal resolution of
$0.93° \times 1.25°$ in the atmosphere (30 levels vertical levels and a finite volume core) and land, and a nominal 1°
resolution in the ocean (60 vertical levels) and sea-ice models with a grid reflecting a displaced North Pole. Both the
LIG and PI experiments are an equilibrium simulations. The LIG simulation represents conditions at 127 ka, the
timing of maximum positive anomaly in Northern Hemisphere insolation. It is forced with changes in atmospheric

100   greenhouse-gas values (275 ppm CO_2, 685 ppb CH_4 and 255 ppb N_2O) and in the orbital parameters (eccentricity =
0.039378, obliquity = 24.040° and perihelion – 180 = 275.41), following Otto-Bliesner et al. (2017). The PI
simulation includes greenhouse and orbital forcing of AD 1850. All other boundary conditions, such as the land-sea
mask, continental ice sheets, and vegetation are the same in the PI and LIG simulations. From the last 20 years of
multi-centennial equilibrium simulation of the PI and of the LIG, we save 6-hourly values of sea-level pressure and

105   of zonal and meridional wind speed at 10 m elevation, i.e., u10 and v10. These values constitute input in the next
modeling step.

2.2   Hydrodynamic simulations

We use the atmospheric outputs from the climate model to force the Global Tide and Surge Model Version 3.0
(GTSMv3.0). GTSM is a depth-averaged hydrodynamic model with global coverage. The model uses the Delft3D

110   Flexible Mesh software (Kernkamp et al., 2011), and has a spatially varying resolution that ranges from 50 km in the
deep ocean to 2.5 km along the coast. The Charnock (1955) relation with a drag coefficient of 0.0041 is used to
estimate the wind stress at the ocean surface. A combination of different datasets is used for the bathymetry:
EMODnet at 250 m resolution around Europe (Consortium_EMODnet_Bathymetry, 2018) and the General
Bathymetric Chart of the Ocean with 30 arc seconds resolution for the rest of the globe (GEBCO, 2014). The

115   bathymetry under the permanent ice shelves in Antarctica is represented by Bedmap2 (Fretwell et al., 2013). For
further details, see Muis et al. (2020) and Wang et al. (2021). We execute GTSM including only storm-surge
processes and exclude astronomical tidal forcing. Time series of surge levels are stored at a 10-minute temporal

resolution for 23,815 output locations. This set of locations was developed by Muis et al. (2020), and includes output every 25-50 km along the global coast. We note that results in the extra-tropical latitudes must be considered more reliable that in the tropics. This is because the spatial resolution of the climate forcing does not allow GTSM to simulate tropical cyclones with realistic frequency and magnitude (Roberts et al., 2020).

2.3 Analysis

In the analysis of the modeling results, we consider seasons separately, except otherwise noted: December-January-February (DJF), March-April-May (MAM), June-July-August (JJA), and September-October-November (SON). To adequately compare seasonal results between the LIG and PI periods, we account for the effect of changes in the earth's orbit across geological time upon the definition of seasons, and we apply the angular (i.e., celestial) definition of calendar (Bartlein and Shafer, 2019). For variables from the climate model simulations - sea level pressure, meridional and zonal wind speed, absolute wind speed - we calculate the climatological average and the seasonal maxima and minima of values sustained for 1-day, 2-days, 3-days and 5-days. To obtain a proxy of surface storminess, we calculate eddy kinetic energy (EKE) from the zonal (u) and meridional (v) wind speeds at 10 m, by filtering out frequencies outside of the 2.5-6 day interval with a Butterworth passband filter, as in, e.g., Pfleiderer et al. (2019). From the value of sea levels resulting from storm surges along the global coastline, we subtracted values of the local sea level averaged across the whole PI and LIG simulations, as these are slightly different between simulations (Fig. S1). We then calculate extreme values of sea levels for several return periods (from 2-year to 20-year), based on seasonal maxima of daily maxima. The calculation of extreme values of sea levels for different return periods is based on the Weibull formula for plotting positions (e.g., Makkonen, 2006):

$$RP = (n+1)/m \qquad (1)$$

Where *RP* is the return period (in years) of the event with rank *m* in the ordered annual/seasonal maxima time series of length *n*. We do not fit extreme value distributions to the maxima and extrapolate values along fitted curves. This approach is adequate since we only consider anomalies in return periods from 2-year to 20-year, a period which is encompassed by the length of our time series.

To estimate the uncertainty around the estimated values for the various return periods of sea level extremes, we use bootstrapping with 599 repetitions to obtain the 5% and 95% confidence bounds (Wilcox, 2010).

3 Results

3.1 Atmospheric variables

The most notable anomalies in sea level pressure between the LIG and the PI climate simulations occur during JJA (Fig. 1). Both seasonal mean and seasonal minimum LIG values are then much lower over Northern Africa, Europe, Central and Northern Asia, and secondarily over Northern America; and much higher over the northernmost sector

150   of the Pacific Ocean. Across all seasons, seasonal LIG minima of sea level pressure deviate from the PI more
       strongly than seasonal means of sea level pressure.

       In the LIG climate simulation, the boundary between westerly and easterly winds of the boreal mid-latitudes slightly
       shifts poleward during JJA (Fig. S2). Conversely, it shifts equatorward during DJF. Further, LIG equatorial
       easterlies during JJA are weaker over the Atlantic and stronger over the western Pacific Ocean sectors. Meridional
155   wind patterns show that LIG Atlantic circulation is on average more zonal during JJA, and slightly less zonal during
       DJF (Fig. S3). Several other seasonal anomalies in zonal and meridional winds speed emerge that we do not mention
       here.

       Atmospheric storminess, as portrayed by EKE, is strongest over the Southern Ocean and oceanic sectors to its north,
       over the northern Pacific and Atlantic Oceans, and over the Arctic Ocean, with substantial seasonal differences.
160   While these broad patterns apply both to the LIG simulation (Fig. 2A) and to the PI simulation (not shown), strong
       seasonal anomalies in EKE emerge over oceanic sectors adjacent to coastal areas, where anomalies have potential
       implications for extreme sea levels. These are mainly the extratropical north Atlantic Ocean, the northwestern and
       northeastern Pacific Ocean, the southern Indian Ocean, and the southeastern Atlantic Ocean.

       ### 3.2 Sea level extremes

165   In the following, we present and discuss sea level extremes due to storm surges, modeled with GTSM, at the return
       period of 10-year as generally representative of extremes at return periods between 2-year and 20-year (shown in
       Fig. S4-S6). In both simulations of the LIG (Fig. 3) and of the PI (not shown), the highest values of extreme sea
       levels are reached at the coast of Northern Europe, northern North America, northern Asia, and at the Gulf of
       Carpentaria in northern Australia (especially during DJF and MAM), of Patagonia and, secondarily, of southern
170   Australia (especially during MAM and JJA) and of the northern Persian Gulf (especially during JJA and SON). The
       high values in these regions are linked to the presence of a wide and shallow continental shelf combined with the
       season of higher storminess.

       Figure 4 maps the significant anomalies in sea level extremes, expressed both in absolute value and as a percentage.
       Anomalies are significant at the 95th confidence level in 8.5% of locations for DJF, in 9.6% for MAM, in 29.5% for
175   JJA, in 8.4% for SON. Annual anomalies are significant in 9.9% of locations (Fig. 5). Considerably higher LIG
       surge levels, i.e., positive anomalies, emerge: in the area of the Gulf of Carpentaria (northern Australia) and parts of
       Indonesia, with anomalies around +0.6 m during DJF; the Mediterranean Sea and northern Africa, with anomalies
       up to +0.2 m during JJA, representing about +100% increase from PI values; around the area of the Gulf of Saint
       Lawrence in northeast America with MAM anomalies that reach +0.4 m, corresponding to about +50%; at the
180   Persian Gulf, with JJA anomalies up to +0.5 m, corresponding to +80%; at the coast of Pakistan and northwest
       India, with SON anomalies up to +0.4 m, corresponding to more than +100%. Considerable negative anomalies are
       found: at the Baltic and North Seas, with anomalies around -0.3 m, with the most profound decrease during DJF; at
       the Bay of Bengal, with DJF anomalies reaching -0.4 m, corresponding to -80%; at the coast of China and Vietnam,
       with JJA anomalies reaching -0.5 m, corresponding to around -60%. Across a large number of islands of the Pacific

185 Ocean and of the Caribbean, significant anomalies are modest in absolute values, but reach around +100% during
DJF and MAM over the Pacific, +60% during JJA over the Caribbean, and -50% during JJA, albeit in different
ocean sectors.

3.3 Correspondence between anomalies in atmospheric variables and sea level extremes

Our results reveal widespread coherence between anomalies of atmospheric storminess and of sea level extremes at
190 the coast (Fig. 2 and 4). Typically, higher LIG EKE values coincide with higher LIG sea level extremes in adjacent
coastlines, and conversely. During DJF, lower LIG EKE values coincide with lower LIG sea level extremes: over a
vast area of the Norwegian, North and Baltic Seas, over the western North Atlantic, Gulf of Mexico and the
Caribbean Sea, and over the Bay of Bengal. Conversely, higher LIG EKE values coincide with higher LIG sea level
extremes over the area of the Indonesian archipelago and northern Australia. During MAM, higher LIG EKE values
195 coincide with higher LIG sea level extremes: over the western North Atlantic, over the western South Atlantic, over
parts of the tropical western Pacific Ocean. During JJA, higher LIG EKE values coincide with higher LIG sea level
extremes: in the Indian Ocean sector around southeastern Africa and Mozambique, over the northeastern sector of
the Pacific Ocean, over parts of the northern Indian Ocean, the Persian Gulf, Red Sea and parts of the Mediterranean
Sea. Conversely, lower LIG EKE values coincide with lower LIG sea level extremes over the northeastern and
200 western sectors of the northern Pacific Ocean. During SON, higher LIG EKE values coincide with higher LIG sea
level extremes: in the Indian Ocean sector around southeastern Africa and Mozambique, over parts of Indonesian
archipelago and in parts of the Caribbean Sea. Conversely, lower LIG EKE values coincide with lower LIG sea level
extremes over parts of the South and East China Sea, and over parts of northwestern Europe.

Coherence between anomalies of sea level pressure and of sea level extremes. Across seasons, negative LIG
205 anomalies of minima of sea-level pressure often correspond with sea-level extremes higher in the LIG than in the PI
(Fig. 1B and 4). This holds true: during JJA, over the Mediterranean, northern Africa and Arabian Peninsula, the
eastern coast of North America, the Caribbean Islands, the Persian Gulf, Mozambique and Madagascar; during
MAM, over the area of the Gulf of Saint Lawrence; and, during DJF, over northern Australia and Indonesia.
Conversely, lower LIG sea-level extremes often coincide with areas where LIG seasonal pressure minima are
210 higher. There are clear deviations from this anti-correlation: e.g., during JJA, over northern Europe; during SON, at
the coast of Pakistan and northwest India; during JJA, over parts of the eastern Indian Ocean and Indonesia.

Clear links do not emerge between anomalies of zonal or meridional wind speeds and of sea level extremes. As an
exception, during JJA, the latitudinal position of maximum intensity of the LIG easterlies over the Caribbean Sea
shifts northwards, coinciding with higher LIG sea level extremes.

215

4 Discussion

In some regions, sea level extremes from storm surges in the LIG and PI climates generally differ from those
modeled for the recent decades by Muis et al. (2016), based on climate reanalysis (Fig. S7): they are higher than the

recent decades in Patagonia, in the Gulf of Carpentaria, and they are lower than recent decades at some coasts of South Asia. Anomalies between LIG and PI are larger than between projected warmer climate of the late 21st century and the recent decades, as modeled by Muis et al. (2020) and Vousdoukas et al. (2018). Nevertheless, the validity of a comparison with those studies is limited by differences in the climate models and reference climate benchmarks employed, such that it is not possible to separate the effect of differences in climate forcing and of different models. More in general, a comparison of surges between the LIG and possible futures has to take into account fundamental differences in the forcing of the two climates: the LIG deviates from the PI due to higher boreal summer insolation, and the future deviates from the PI and the modern climate due to higher greenhouse gas concentration. On the other hand, spatial patterns of warming during JJA in the Northern Hemisphere are similar across simulations of the LIG and of warmer futures, as evident from the fact that boreal summer sea surface temperature patterns in the LIG simulation somewhat resemble those of the projected futures (Fig. S8). A qualitative comparison of results for the summer of the Northern Hemisphere is therefore meaningful. It is important to note, in this context, that it is during JJA that the largest values are reached in anomalies of temperature (Fig. S8; see also Otto-Bliesner et al. (2021)), and also of sea level extremes (Fig. 4), when anomalies are significant in three times as many locations as for the other seasons (29.5% of locations).

4.1 Implication for paleo sea level proxies

Our results have implications also on the interpretation of certain geological facies that are used to reconstruct LIG relative sea level, i.e., the local absolute elevation of paleo sea level, still uncorrected for post-depositional effects such as due to Glacial Isostatic Adjustment and tectonics. Reconstructions of paleo relative sea level from field data often use the uniformitarianism approach, i.e., the assumption that processes acted essentially with the same intensity in the past as they do in the present (Lyell, 1830). In the practice of sea level reconstruction, this concept often entails using modern analogs to calculate the relationship between the measured elevation of a paleo relative sea level proxy and the paleo sea level. Different levels attained by storm surges in the LIG might affect the interpretation of wave-built relative sea level proxies such as beach deposits or beach ridges. Beach ridges are widespread along the Atlantic coasts of South America (Patagonia) and the Gulf Coast of the U.S. (Gowan et al., 2021; Simms, 2021). In our models, both areas show variations in the order of up to a few tens of centimeters in the LIG annual sea level extremes, which do not reach statistical significance (Fig. 5). LIG beach deposits are instead widely distributed globally, and our results contain annual anomalies that reach multiple tens of centimeters at several other locations, e.g., in the Western Mediterranean (Cerrone et al., 2021). We surmise that it may be possible that, at these locations, the uniformitarianism principle may not be directly applicable to beach deposits and beach ridges. For proxies correlated to LIG extreme storm deposits, like those reported in Bermuda and the Bahamas (Hearty, 1997; Hearty et al., 1998; Hearty and Tormey, 2017), our results may help disentangle in which areas it may be of interest to combine our storm surge models with wave modeling, to unravel whether higher surges may have also been coupled with higher waves.

4.2 Limitations and future research

It is known that the modelling of extreme sea levels based on global climate models is prone to large spatial biases
(Muis et al., 2020). While regional studies have attempted to correct for such biases (Marsooli et al., 2019), global
studies have not. However, if we assume biases to equally affect the PI and the LIG simulations, the anomalies
between results based on the two simulations, which we report here, should not be impacted by the presence of
biases. Nevertheless, there are considerable uncertainties associated with the meteorological forcing that we use
here, and there are several research directions that could be explored in future research. First, the resolution of the
CESM1.2 model, although high in the context of state-of-the-art GCMs, is not fully storm-resolving. Higher
resolution would improve spatial gradients in pressure and wind speeds, and much increase the representation of
tropical storms. Second, the length of the GCM simulations (20 years) is relatively short for assessing changes in the
probabilities of extremes, especially on account of the large internal variability. Increasing the length of the
simulations would make the detection of changes in extreme value statistics more robust. Third, future research
should account for the model bias and uncertainty by performing hydrodynamic simulations based on an ensemble
of climate models, such as the ensemble of LIG experiments analyzed in Otto-Bliesner et al. (2021). Higher
confidence could be placed on anomalies in LIG storm surges that emerge as robust across the ensemble.

An important assumption that underlies our analysis is that we only consider climatic changes and do not account
for changes in mean sea level that originate from different extents of polar ice sheets and from steric processes. The
generation of a storm surge is influenced by changes in bathymetry, coastal geometry, and geomorphic features such
as river deltas, barrier islands, and bays, which all interact and can modulate the height of the storm surge (Islam et
al., 2021). Moreover, storm surges are influenced by variations in water depth as well as the sea-air momentum
exchange, and as such they can be modulated by (non-linear) interaction effects with tides and waves (Idier et al.,
2019). This has been shown in regional studies that use fully coupled hydrodynamic models, such as Arns et al.
(2017). At the global scale, interaction effects are typically excluded and considered to be negligible compared to
the other sources of uncertainty (Dullaart et al., 2020; Vousdoukas et al., 2018), although Arns et al. (2020) have
used statistical modelling to show that interaction effects can modulate extreme sea levels. The starkly different
climate of the LIG, however, warrants exploration of this set of interactions, which could be accomplished by: 1)
including LIG mean sea level anomalies such as resulting from a GIA modeling approach and from inclusion of
steric effects and changes in ocean circulation; 2) running GTSM simulations, with inclusion of such mean sea level
anomalies with activation of the tidal component of the model; and 3) including wave modeling, globally or for
specific regions of interest. This is computationally expensive, but it seems like the near-ideal approach to
investigate drivers behind observed changes at key paleo sea level indicators sites.

5 Conclusions

We report the first results of simulations of storm surge under climatic conditions representing the Last Interglacial
and the pre-industrial periods. These reveal that a naturally (orbitally) forced warmer climate implies significant
seasonal and annual anomalies in sea level extremes along the coastline of many global areas. Those anomalies can
be linked to changes in patterns of atmospheric storminess in our climate simulations. For some locations, anomalies

of sea level extremes reach multiple tens of centimeters, and are considerable in terms of percentage change. These
290   insights can inform the interpretation of existing and upcoming future paleo sea level indicators. Lastly, we suggest
research avenues to improve the realism of modeled sea level extremes for the LIG by including other relevant
processes in the modeling framework.

Author contribution

PS, SM, AR, PJW and JCJHA designed the study. PB carried out the climate model simulations. JD and SM carried
295   out the hydrodynamic simulations. PS and JD processed and analyzed the datasets. PS prepared the figures. PS, SM
and AR lead the writing of the manuscript. All authors contributed to the interpretation of results and writing of the
manuscript.

Competing interests

300   Some authors are members of the editorial board of Climate of the Past. The peer-review process was guided by an
independent editor, and the authors have no other competing interests to declare.

Acknowledgements

We acknowledge funding from SCOR under project COASTRISK; from NWO (Nederlandse Organisatie voor
305   Wetenschappelijk Onderzoek) under grant ALWOP.164 (P. Scussolini), under grant ASDI.2018.036 (MOSAIC
project; S. Muis), and under NWO-VICI grant 453-13-006 (J.C.J.H. Aerts); from the European Research Council
(ERC), under the European Union's Horizon 2020 Programme for Research and Innovation grant 802414 (A.
Rovere), and under advanced grant 884442 (J.C.J.H. Aerts).

310   **References**

Arns, A., Dangendorf , S., Jensen, J., Talke, S., Bender, J., Pattiaratchi, C., 2017. Sea-level rise induced
amplification of coastal protection design heights. Scientific Reports 7, 40171.

Arns, A., Wahl, T., Wolff, C., Vafeidis, A.T., Haigh, I.D., Woodworth, P., Niehüser, S., Jensen, J., 2020.
Non-linear interaction modulates global extreme sea levels, coastal flood exposure, and impacts. Nature
315   Communications 11, 1918.

Bartlein, P.J., Shafer, S.L., 2019. Paleo calendar-effect adjustments in time-slice and transient climate-
model simulations (PaleoCalAdjust v1.0): impact and strategies for data analysis. Geosci. Model Dev. 12,
3889-3913.

Belmonte Rivas, M., Stoffelen, A., 2019. Characterizing ERA-Interim and ERA5 surface wind biases
320   using ASCAT. Ocean Sci. 15, 831-852.

Bindoff, N.L., W.W.L. Cheung, J.G. Kairo, J. Arístegui, V.A. Guinder, R. Hallberg, N. Hilmi, N. Jiao,
M.S. Karim, L. Levin, S. O'Donoghue, S.R. Purca Cuicapusa, B. Rinkevich, T. Suga, A. Tagliabue, and
P. Williamson, 2019. Changing Ocean, Marine Ecosystems, and Dependent Communities, in: H.-O.

Pörtner, D.C.R., V. Masson-Delmotte, P. Zhai, M. Tignor, E. Poloczanska, K. Mintenbeck, A. Alegría, M. Nicolai, A. Okem, J. Petzold, B. Rama, N.M. Weyer (Ed.), IPCC Special Report on the Ocean and Cryosphere in a Changing Climate, In press.

CAPE_Members, 2006. Last Interglacial Arctic warmth confirms polar amplification of climate change. Quaternary Science Reviews 25, 1383-1400.

Catto, J.L., Ackerley, D., Booth, J.F., Champion, A.J., Colle, B.A., Pfahl, S., Pinto, J.G., Quinting, J.F., Seiler, C., 2019. The Future of Midlatitude Cyclones. Current Climate Change Reports 5, 407-420.

Cerrone, C., Vacchi, M., Fontana, A., Rovere, A., 2021. Last Interglacial sea-level proxies in the Western Mediterranean. Earth Syst. Sci. Data Discuss. 2021, 1-93.

Chang, E.K.M., Guo, Y., Xia, X., 2012. CMIP5 multimodel ensemble projection of storm track change under global warming. Journal of Geophysical Research: Atmospheres 117.

Charnock, H., 1955. Wind stress on a water surface. Quarterly Journal of the Royal Meteorological Society 81, 639-640.

Consortium_EMODnet_Bathymetry, 2018. EMODnet Digital Bathymetry (DTM).

Dullaart, J.C.M., Muis, S., Bloemendaal, N., Aerts, J.C.J.H., 2020. Advancing global storm surge modelling using the new ERA5 climate reanalysis. Climate Dynamics 54, 1007-1021.

Dutton, A., Carlson, A.E., Long, A.J., Milne, G.A., Clark, P.U., DeConto, R., Horton, B.P., Rahmstorf, S., Raymo, M.E., 2015a. Sea-level rise due to polar ice-sheet mass loss during past warm periods. Science 349, aaa4019.

Dutton, A., Webster, J.M., Zwartz, D., Lambeck, K., Wohlfarth, B., 2015b. Tropical tales of polar ice: evidence of Last Interglacial polar ice sheet retreat recorded by fossil reefs of the granitic Seychelles islands. Quaternary Science Reviews 107, 182-196.

Dyer, B., Austermann, J., D'Andrea, W.J., Creel, R.C., Sandstrom, M.R., Cashman, M., Rovere, A., Raymo, M.E., 2021. Sea-level trends across The Bahamas constrain peak last interglacial ice melt. Proceedings of the National Academy of Sciences 118, e2026839118.

Enríquez, A.R., Wahl, T., Marcos, M., Haigh, I.D., 2020. Spatial Footprints of Storm Surges Along the Global Coastlines. Journal of Geophysical Research: Oceans 125, e2020JC016367.

Francis, J., Skific, N., 2015. Evidence linking rapid Arctic warming to mid-latitude weather patterns. Philosophical Transactions of the Royal Society A: Mathematical, Physical and Engineering Sciences 373, 20140170.

Fretwell, P., Pritchard, H.D., Vaughan, D.G., Bamber, J.L., Barrand, N.E., Bell, R., Bianchi, C., Bingham, R.G., Blankenship, D.D., Casassa, G., Catania, G., Callens, D., Conway, H., Cook, A.J., Corr, H.F.J., Damaske, D., Damm, V., Ferraccioli, F., Forsberg, R., Fujita, S., Gim, Y., Gogineni, P., Griggs, J.A., Hindmarsh, R.C.A., Holmlund, P., Holt, J.W., Jacobel, R.W., Jenkins, A., Jokat, W., Jordan, T., King, E.C., Kohler, J., Krabill, W., Riger-Kusk, M., Langley, K.A., Leitchenkov, G., Leuschen, C., Luyendyk, B.P., Matsuoka, K., Mouginot, J., Nitsche, F.O., Nogi, Y., Nost, O.A., Popov, S.V., Rignot, E., Rippin, D.M., Rivera, A., Roberts, J., Ross, N., Siegert, M.J., Smith, A.M., Steinhage, D., Studinger, M., Sun, B., Tinto, B.K., Welch, B.C., Wilson, D., Young, D.A., Xiangbin, C., Zirizzotti, A., 2013. Bedmap2: improved ice bed, surface and thickness datasets for Antarctica. The Cryosphere 7, 375-393.

GEBCO, 2014. General Bathymetric Chart of the Oceans (GEBCO) 2014 Grid.

Gowan, E.J., Rovere, A., Ryan, D.D., Richiano, S., Montes, A., Pappalardo, M., Aguirre, M.L., 2021. Last interglacial (MIS 5e) sea-level proxies in southeastern South America. Earth Syst. Sci. Data 13, 171-197.

Haarsma, R.J., Hazeleger, W., Severijns, C., de Vries, H., Sterl, A., Bintanja, R., van Oldenborgh, G.J., van den Brink, H.W., 2013. More hurricanes to hit western Europe due to global warming. Geophysical Research Letters 40, 1783-1788.

370 Hansen, J., Sato, M., Hearty, P., Ruedy, R., Kelley, M., Masson-Delmotte, V., Russell, G., Tselioudis, G., Cao, J., Rignot, E., Velicogna, I., Tormey, B., Donovan, B., Kandiano, E., von Schuckmann, K., Kharecha, P., Legrande, A.N., Bauer, M., Lo, K.-W., 2016. Ice melt, sea level rise and superstorms: evidence from paleoclimate data, climate modeling, and modern observations that 2 °C global warming could be dangerous. Atmospheric Chemistry and Physics 16, 3761-3812.

375 Harvey, B.J., Cook, P., Shaffrey, L.C., Schiemann, R., 2020. The Response of the Northern Hemisphere Storm Tracks and Jet Streams to Climate Change in the CMIP3, CMIP5, and CMIP6 Climate Models. Journal of Geophysical Research: Atmospheres 125, e2020JD032701.

Hearty, P.J., 1997. Boulder Deposits from Large Waves during the Last Interglaciation on North Eleuthera Island, Bahamas. Quaternary Research 48, 326-338.

380 Hearty, P.J., Neumann, A.C., Kaufman, D.S., 1998. Chevron Ridges and Runup Deposits in the Bahamas from Storms Late in Oxygen-Isotope Substage 5e. Quaternary Research 50, 309-322.

Hearty, P.J., Tormey, B.R., 2017. Sea-level change and superstorms; geologic evidence from the last interglacial (MIS 5e) in the Bahamas and Bermuda offers ominous prospects for a warming Earth. Marine Geology 390, 347-365.

385 Hearty, P.J., Tormey, B.R., 2018. Listen to the whisper of the rocks, telling their ancient story. Proceedings of the National Academy of Sciences 115, E2902-E2903.

Hoffman, J.S., Clark, P.U., Parnell, A.C., He, F., 2017. Regional and global sea-surface temperatures during the last interglaciation. Science 355, 276-279.

Hurrell, J.W., Holland, M.M., Gent, P.R., Ghan, S., Kay, J.E., Kushner, P.J., Lamarque, J.-F., Large,
390 W.G., Lawrence, D., Lindsay, K., Lipscomb, W.H., Long, M.C., Mahowald, N., Marsh, D.R., Neale, R.B., Rasch, P., Vavrus, S., Vertenstein, M., Bader, D., Collins, W.D., Hack, J.J., Kiehl, J., Marshall, S., 2013. The Community Earth System Model: A Framework for Collaborative Research. Bulletin of the American Meteorological Society 94, 1339-1360.

Idier, D., Bertin, X., Thompson, P., Pickering, M.D., 2019. Interactions Between Mean Sea Level, Tide,
395 Surge, Waves and Flooding: Mechanisms and Contributions to Sea Level Variations at the Coast. Surveys in Geophysics 40, 1603-1630.

Islam, M.R., Lee, C.-Y., Mandli, K.T., Takagi, H., 2021. A new tropical cyclone surge index incorporating the effects of coastal geometry, bathymetry and storm information. Scientific Reports 11, 16747.

400 Jouzel, J., Masson-Delmotte, V., Cattani, O., Dreyfus, G., Falourd, S., Hoffmann, G., Minster, B., Nouet, J., Barnola, J.M., Chappellaz, J., Fischer, H., Gallet, J.C., Johnsen, S., Leuenberger, M., Loulergue, L., Luethi, D., Oerter, H., Parrenin, F., Raisbeck, G., Raynaud, D., Schilt, A., Schwander, J., Selmo, E., Souchez, R., Spahni, R., Stauffer, B., Steffensen, J.P., Stenni, B., Stocker, T.F., Tison, J.L., Werner, M., Wolff, E.W., 2007. Orbital and millennial Antarctic climate variability over the past 800,000 years.
405 Science 317, 793-796.

Kaspar, F., Spangehl, T., Cubasch, U., 2007. Northern hemisphere winter storm tracks of the Eemian interglacial and the last glacial inception. Clim. Past 3, 181-192.

Kernkamp, H.W.J., Van Dam, A., Stelling, G.S., de Goede, E.D., 2011. Efficient scheme for the shallow water equations on unstructured grids with application to the Continental Shelf. Ocean Dynamics 61,
410 1175-1188.

Kirezci, E., Young, I.R., Ranasinghe, R., Muis, S., Nicholls, R.J., Lincke, D., Hinkel, J., 2020. Projections of global-scale extreme sea levels and resulting episodic coastal flooding over the 21st Century. Scientific Reports 10, 11629.

Koh, J.H., Brierley, C.M., 2015. Tropical cyclone genesis potential across palaeoclimates. Clim. Past 11, 1433-1451.

Kopp, R.E., Simons, F.J., Mitrovica, J.X., Maloof, A.C., Oppenheimer, M., 2009. Probabilistic assessment of sea level during the last interglacial stage. Nature 462, 863-867.

Lunt, D.J., Elderfield, H., Pancost, R., Ridgwell, A., Foster, G.L., Haywood, A., Kiehl, J., Sagoo, N., Shields, C., Stone, E.J., Valdes, P., 2013. Warm climates of the past—a lesson for the future? Philosophical Transactions of the Royal Society A: Mathematical, Physical and Engineering Sciences 371.

Lyell, C., Sir., 1830. Principles of geology: being an attempt to explain the former changes of the earth's surface, by reference to causes now in operation.

Makkonen, L., 2006. Plotting Positions in Extreme Value Analysis. Journal of Applied Meteorology and Climatology 45, 334-340.

Marsooli, R., Lin, N., Emanuel, K., Feng, K., 2019. Climate change exacerbates hurricane flood hazards along US Atlantic and Gulf Coasts in spatially varying patterns. Nature Communications 10, 3785.

McKay, N.P., Overpeck, J.T., Otto-Bliesner, B.L., 2011. The role of ocean thermal expansion in Last Interglacial sea level rise. Geophysical Research Letters 38.

Mori, N., Shimura, T., Yoshida, K., Mizuta, R., Okada, Y., Fujita, M., Khujanazarov, T., Nakakita, E., 2019. Future changes in extreme storm surges based on mega-ensemble projection using 60-km resolution atmospheric global circulation model. Coastal Engineering Journal 61, 295-307.

Muis, S., Apecechea, M.I., Dullaart, J., de Lima Rego, J., Madsen, K.S., Su, J., Yan, K., Verlaan, M., 2020. A High-Resolution Global Dataset of Extreme Sea Levels, Tides, and Storm Surges, Including Future Projections. Frontiers in Marine Science 7.

Muis, S., Verlaan, M., Winsemius, H.C., Aerts, J.C., Ward, P.J., 2016. A global reanalysis of storm surges and extreme sea levels. Nat Commun 7, 11969.

Mylroie, J.E., 2008. Late Quaternary sea-level position: Evidence from Bahamian carbonate deposition and dissolution cycles. Quaternary International 183, 61-75.

Mylroie, J.E., 2018. Superstorms: Comments on Bahamian Fenestrae and Boulder Evidence from the Last Interglacial. Journal of Coastal Research 34, 1471-1483, 1413.

Neem_Community_Members, 2013. Eemian interglacial reconstructed from a Greenland folded ice core. Nature 493, 489-494.

Otto-Bliesner, B.L., Brady, E.C., Zhao, A., Brierley, C.M., Axford, Y., Capron, E., Govin, A., Hoffman, J.S., Isaacs, E., Kageyama, M., Scussolini, P., Tzedakis, P.C., Williams, C.J.R., Wolff, E., Abe-Ouchi, A., Braconnot, P., Ramos Buarque, S., Cao, J., de Vernal, A., Guarino, M.V., Guo, C., LeGrande, A.N., Lohmann, G., Meissner, K.J., Menviel, L., Morozova, P.A., Nisancioglu, K.H., O'Ishi, R., Salas y Mélia, D., Shi, X., Sicard, M., Sime, L., Stepanek, C., Tomas, R., Volodin, E., Yeung, N.K.H., Zhang, Q., Zhang, Z., Zheng, W., 2021. Large-scale features of Last Interglacial climate: results from evaluating the lig127k simulations for the Coupled Model Intercomparison Project (CMIP6)–Paleoclimate Modeling Intercomparison Project (PMIP4). Clim. Past 17, 63-94.

Otto-Bliesner, B.L., Rosenbloom, N., Stone, E.J., McKay, N.P., Lunt, D.J., Brady, E.C., Overpeck, J.T., 2013. How warm was the last interglacial? New model–data comparisons. Philosophical Transactions of the Royal Society A: Mathematical, Physical and Engineering Sciences 371.

455 Pfleiderer, P., Schleussner, C.-F., Kornhuber, K., Coumou, D., 2019. Summer weather becomes more persistent in a 2 °C world. Nature Climate Change 9, 666-671.

Raible, C.C., Pinto, J.G., Ludwig, P., Messmer, M., 2021. A review of past changes in extratropical cyclones in the northern hemisphere and what can be learned for the future. WIREs Climate Change 12, e680.

460 Resio, D.T., Westerink, J.J., 2008. Modeling the physics of storm surges. Physics Today 61, 33-38.

Roberts, M.J., Camp, J., Seddon, J., Vidale, P.L., Hodges, K., Vanniere, B., Mecking, J., Haarsma, R., Bellucci, A., Scoccimarro, E., Caron, L.-P., Chauvin, F., Terray, L., Valcke, S., Moine, M.-P., Putrasahan, D., Roberts, C., Senan, R., Zarzycki, C., Ullrich, P., 2020. Impact of Model Resolution on Tropical Cyclone Simulation Using the HighResMIP–PRIMAVERA Multimodel Ensemble. Journal of
465 Climate 33, 2557-2583.

Rohling, E.J., Hibbert, F.D., Grant, K.M., Galaasen, E.V., Irvalı, N., Kleiven, H.F., Marino, G., Ninnemann, U., Roberts, A.P., Rosenthal, Y., Schulz, H., Williams, F.H., Yu, J., 2019. Asynchronous Antarctic and Greenland ice-volume contributions to the last interglacial sea-level highstand. Nature Communications 10, 5040.

470 Rovere, A., Casella, E., Harris, D.L., Lorscheid, T., Nandasena, N.A.K., Dyer, B., Sandstrom, M.R., Stocchi, P., D'Andrea, W.J., Raymo, M.E., 2017. Giant boulders and Last Interglacial storm intensity in the North Atlantic. Proc Natl Acad Sci U S A 114, 12144-12149.

Rovere, A., Casella, E., Harris, D.L., Lorscheid, T., Nandasena, N.A.K., Dyer, B., Sandstrom, M.R., Stocchi, P., D'Andrea, W.J., Raymo, M.E., 2018. Reply to Hearty and Tormey: Use the scientific method to test geologic hypotheses, because rocks do not whisper. Proceedings of the National Academy of
475 Sciences 115, E2904-E2905.

Salonen, J.S., Sánchez-Goñi, M.F., Renssen, H., Plikk, A., 2021. Contrasting northern and southern European winter climate trends during the Last Interglacial. Geology 49, 1220-1224.

Scheffers, A., Kelletat, D., 2020. Megaboulder Movement by Superstorms: A Geomorphological
480 Approach. Journal of Coastal Research 36, 844-856, 813.

Scussolini, P., Bakker, P., Guo, C., Stepanek, C., Zhang, Q., Braconnot, P., Cao, J., Guarino, M.-V., Coumou, D., Prange, M., Ward, P.J., Renssen, H., Kageyama, M., Otto-Bliesner, B., Aerts, J.C.J.H., 2019. Agreement between reconstructed and modeled boreal precipitation of the Last Interglacial. Science Advances 5, eaax7047.

485 Scussolini, P., Eilander, D., Sutanudjaja, E.H., Ikeuchi, H., Hoch, J.M., Ward, P.J., Bakker, P., Otto-Bliesner, B.L., Guo, C., Stepanek, C., Zhang, Q., Braconnot, P., Guarino, M.-V., Muis, S., Yamazaki, D., Veldkamp, T.I.E., Aerts, J.C.J.H., 2020. Global River Discharge and Floods in the Warmer Climate of the Last Interglacial. Geophysical Research Letters 47, luue2020GL089375.

Shackleton, S., Baggenstos, D., Menking, J.A., Dyonisius, M.N., Bereiter, B., Bauska, T.K., Rhodes,
490 R.H., Brook, E.J., Petrenko, V.V., McConnell, J.R., Kellerhals, T., Häberli, M., Schmitt, J., Fischer, H., Severinghaus, J.P., 2020. Global ocean heat content in the Last Interglacial. Nature Geoscience 13, 77-81.

Shaw, T.A., Baldwin, M., Barnes, E.A., Caballero, R., Garfinkel, C.I., Hwang, Y.T., Li, C., O'Gorman, P.A., Rivière, G., Simpson, I.R., Voigt, A., 2016. Storm track processes and the opposing influences of climate change. Nature Geoscience 9, 656-664.

495 Simms, A.R., 2021. Last interglacial sea levels within the Gulf of Mexico and northwestern Caribbean Sea. Earth Syst. Sci. Data 13, 1419-1439.

Staten, P.W., Lu, J., Grise, K.M., Davis, S.M., Birner, T., 2018. Re-examining tropical expansion. Nature Climate Change 8, 768-775.

500 Takahashi, H., Su, H., Jiang, J.H., 2016. Water vapor changes under global warming and the linkage to present-day interannual variabilities in CMIP5 models. Climate Dynamics 47, 3673-3691.

Turney, C.S.M., Fogwill, C.J., Golledge, N.R., McKay, N.P., van Sebille, E., Jones, R.T., Etheridge, D., Rubino, M., Thornton, D.P., Davies, S.M., Ramsey, C.B., Thomas, Z.A., Bird, M.I., Munksgaard, N.C., Kohno, M., Woodward, J., Winter, K., Weyrich, L.S., Rootes, C.M., Millman, H., Albert, P.G., Rivera, A., van Ommen, T., Curran, M., Moy, A., Rahmstorf, S., Kawamura, K., Hillenbrand, C.-D., Weber,
505 M.E., Manning, C.J., Young, J., Cooper, A., 2020a. Early Last Interglacial ocean warming drove substantial ice mass loss from Antarctica. Proceedings of the National Academy of Sciences, 201902469.

Turney, C.S.M., Jones, R., McKay, N.P., van Sebille, E., Thomas, Z.A., Hillenbrand, C.D., Fogwill, C.J., 2020b. A global mean sea-surface temperature dataset for the Last Interglacial (129-116 kyr) and contribution of thermal expansion to sea-level change. Earth Syst. Sci. Data Discuss. 2020, 1-21.

510 Turney, C.S.M., Jones, R.T., 2010. Does the Agulhas Current amplify global temperatures during super-interglacials? Journal of Quaternry Science 25, 839-843.

Vimpere, L., Kindler, P., Castelltort, S., 2019. Chevrons: Origin and relevance for the reconstruction of past wind regimes. Earth-Science Reviews 193, 317-332.

Vousdoukas, M.I., Mentaschi, L., Voukouvalas, E., Verlaan, M., Jevrejeva, S., Jackson, L.P., Feyen, L.,
515 2018. Global probabilistic projections of extreme sea levels show intensification of coastal flood hazard. Nature Communications 9, 2360.

Wang, X., Verlaan, M., Apecechea, M.I., Lin, H.X., 2021. Computation-Efficient Parameter Estimation for a High-Resolution Global Tide and Surge Model. Journal of Geophysical Research: Oceans 126, e2020JC016917.

520 Wilcox, R.R., 2010. The Bootstrap, Fundamentals of Modern Statistical Methods: Substantially Improving Power and Accuracy. Springer New York, New York, NY, pp. 87-108.

Yamada, Y., Satoh, M., Sugi, M., Kodama, C., Noda, A.T., Nakano, M., Nasuno, T., 2017. Response of Tropical Cyclone Activity and Structure to Global Warming in a High-Resolution Global Nonhydrostatic Model. Journal of Climate 30, 9703-9724.

525 Yan, Q., Korty, R., Wei, T., Jiang, N., 2021. A Westward Shift in Tropical Cyclone Potential Intensity and Genesis Regions in the North Atlantic During the Last Interglacial. Geophysical Research Letters 48, e2021GL093946.
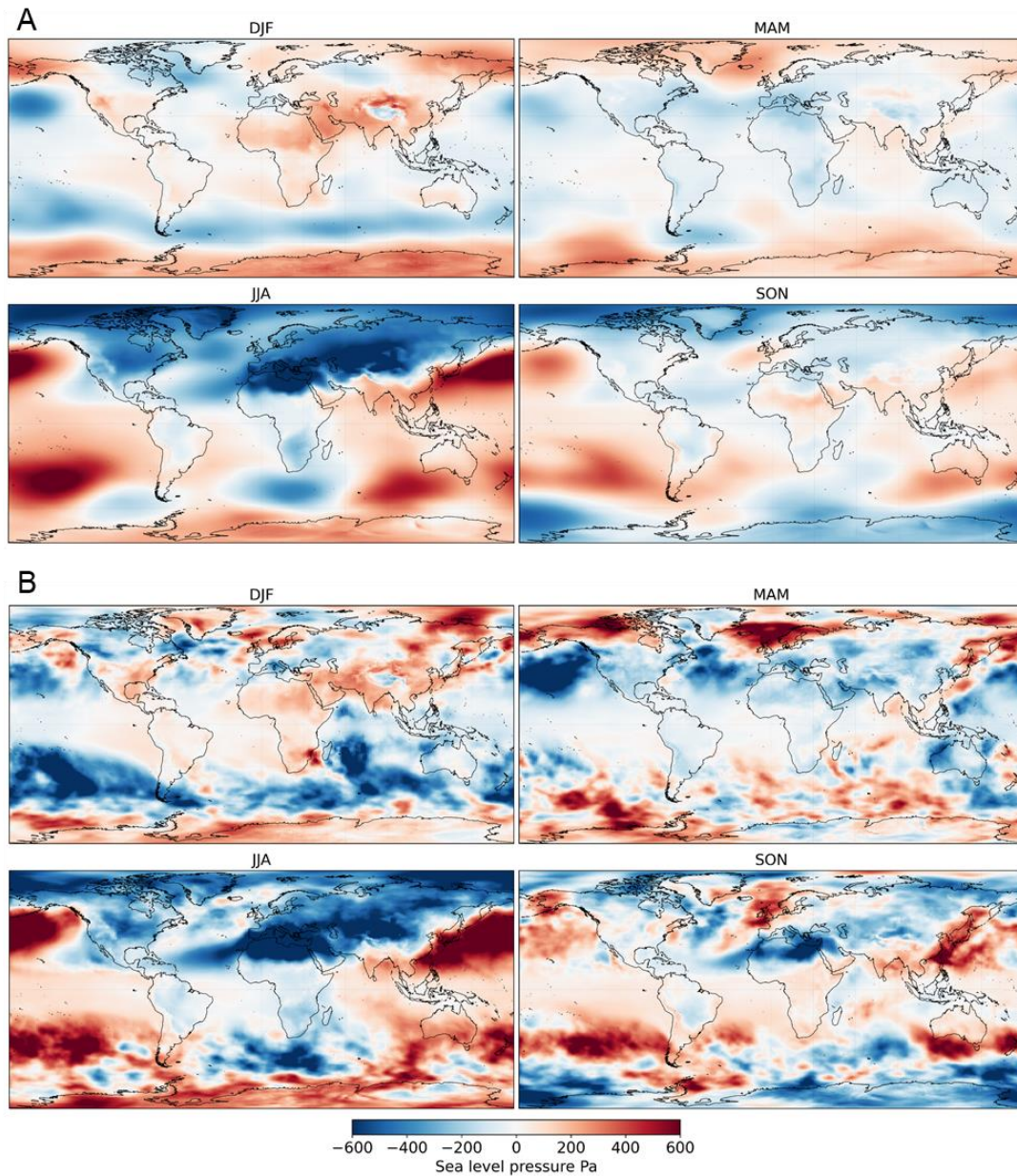
Figure 1. Anomalies (LIG-PI) in sea-level pressure. A) seasonal mean; B) seasonal daily minimum. DJF indicates months December-January-February, and so on.
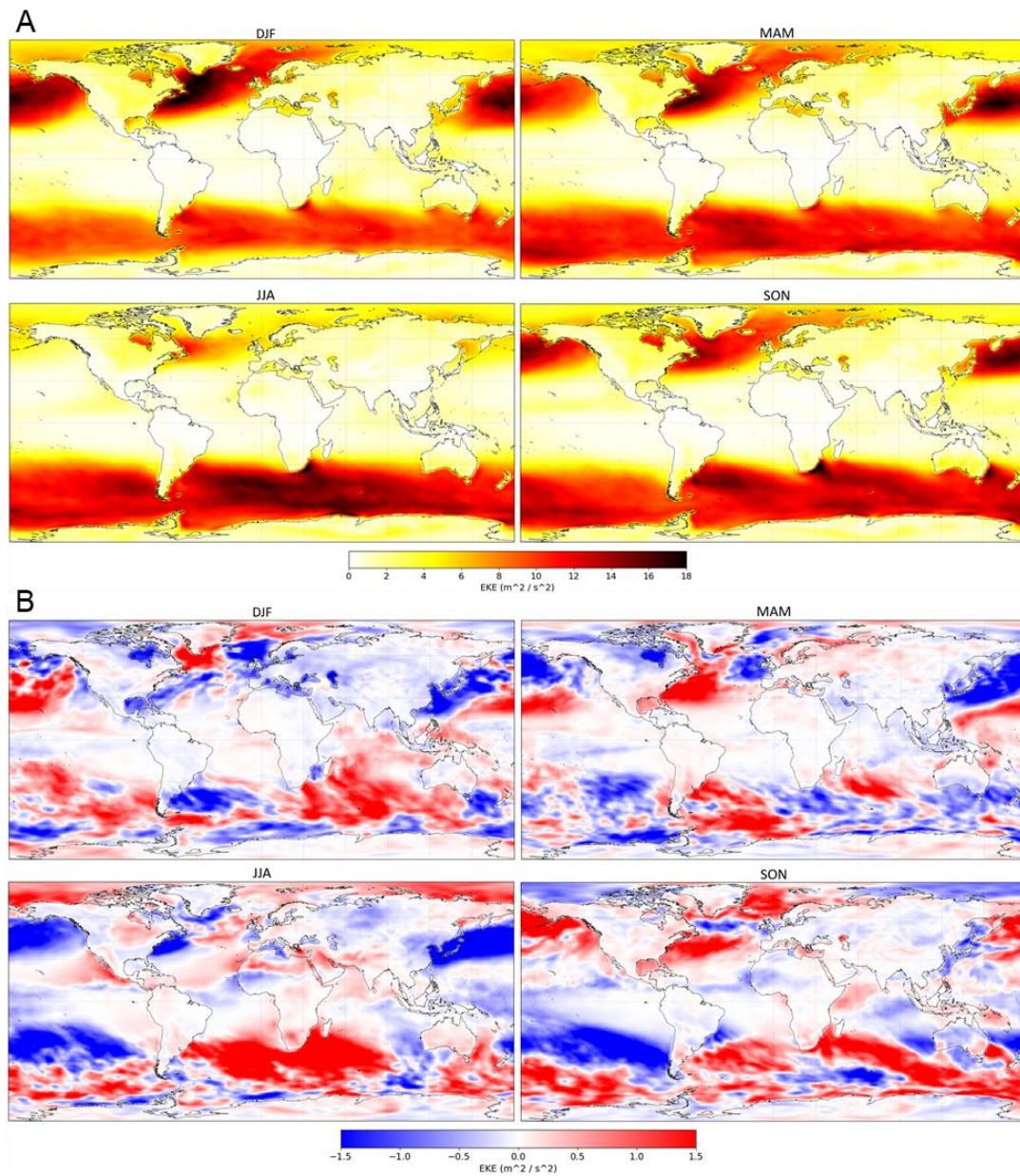
Figure. 2. A) Eddy kinetic energy (EKE), calculated from zonal and meridional wind speeds (see Methods), in the LIG simulation. B) EKE anomalies (LIG-PI).
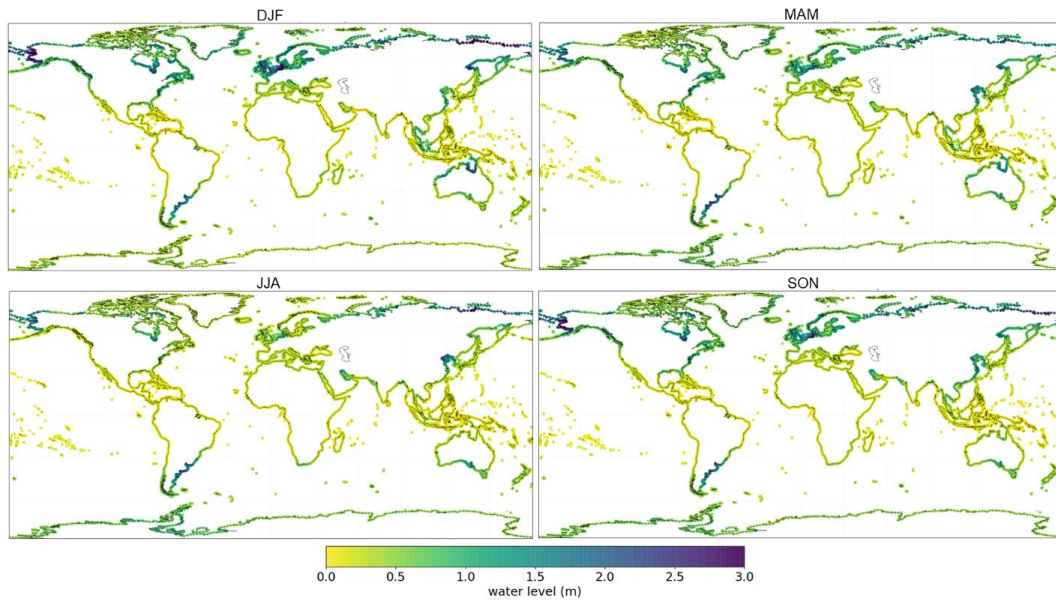
535

Fig. 3. Sea level extremes from storm surges in the LIG simulation, at the 10-year return period.
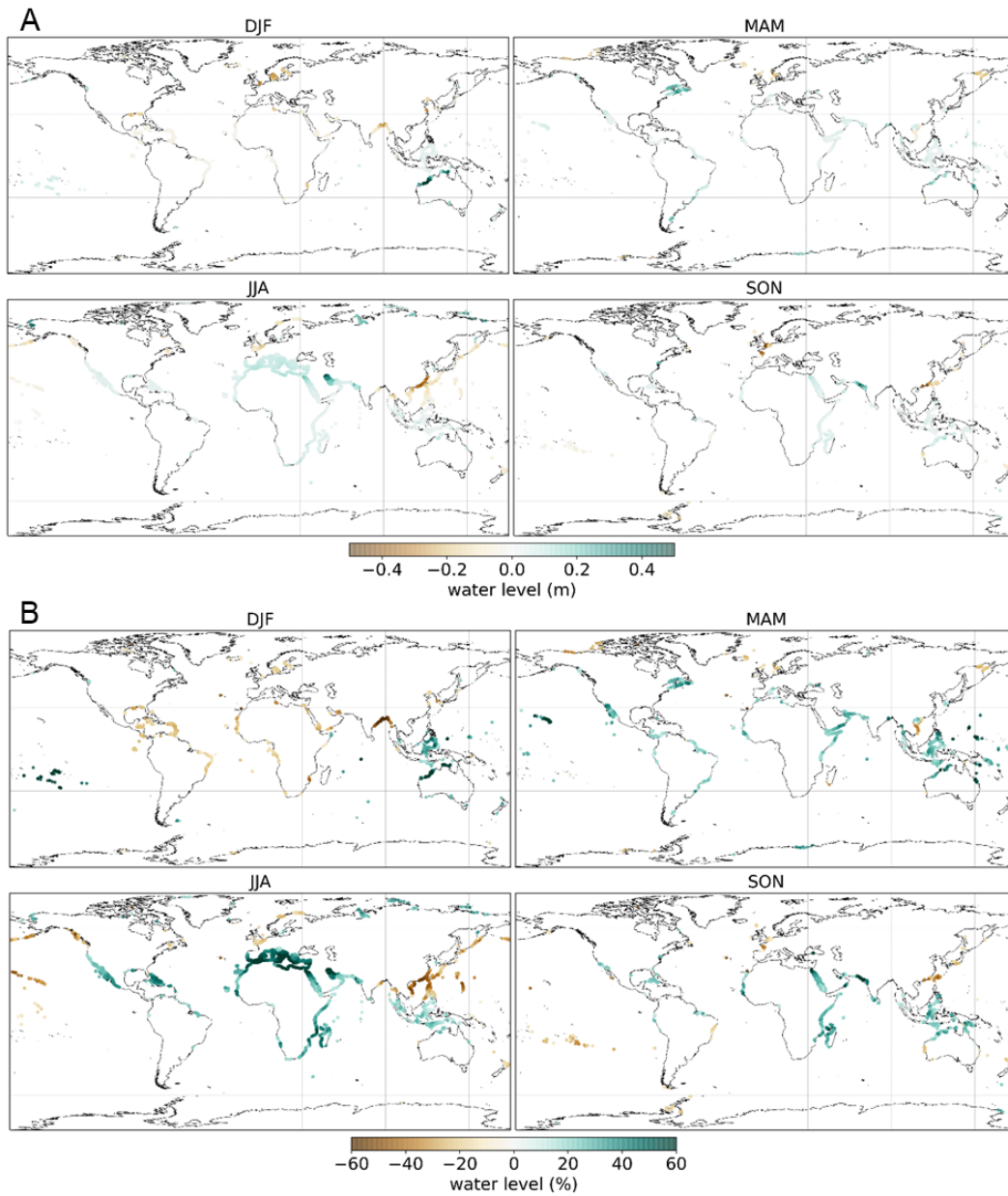
Fig. 4. Anomalies (LIG-PI) in sea level extremes at the 10-year return period, as A) absolute, and B) as percentage values.

Only values for which the 95% uncertainty bands of the distributions of each climate do not overlap.
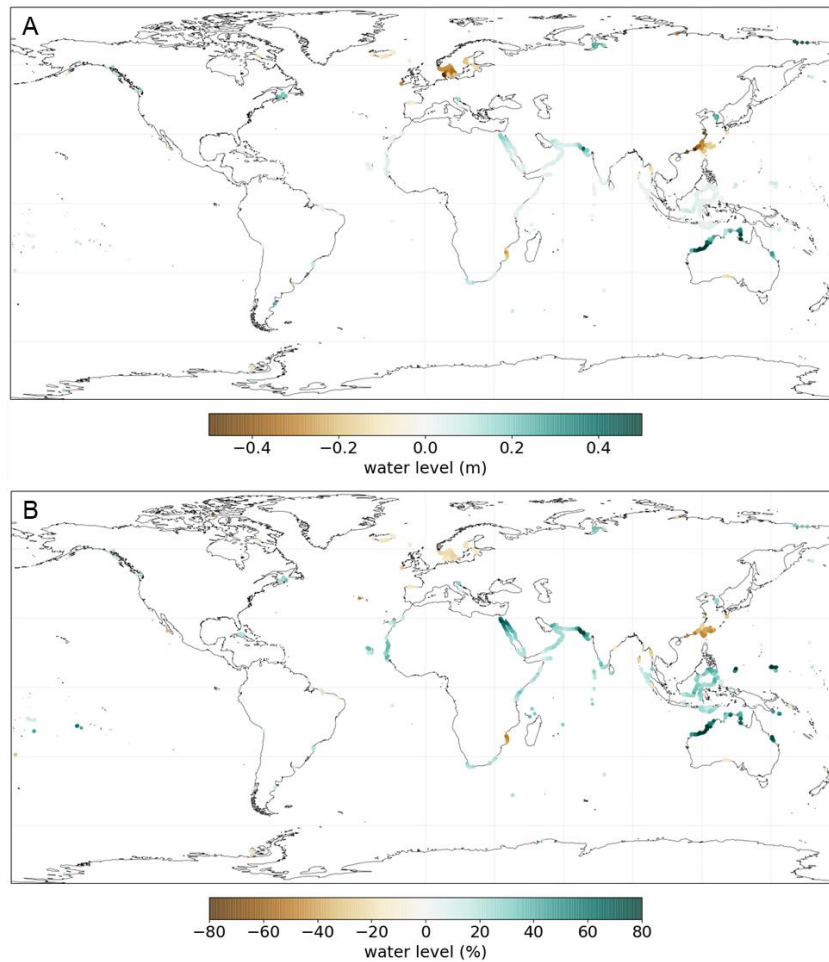
540

Fig. 5. Same as Fig. 4, but for annual instead of seasonal anomalies in sea level extremes.